

360° Panorama Cloning on Sphere

Qiang Zhao^{1,2}, Liang Wan^{2†}, Wei Feng³, Jiawan Zhang², Tien-Tsin Wong⁴

¹Institute of Computing Technology, Chinese Academy of Sciences, China

²School of Computer Software, Tianjin University, China

³School of Computer Science and Technology, Tianjin University, China

⁴Dept. of Computer Science and Engineering, The Chinese University of Hong Kong

Abstract

In this paper, we address a novel problem of cloning a patch of the source spherical panoramic image to the target spherical panoramic image, which we call 360° panorama cloning. Considering the sphere geometry constraint embedded in spherical panoramic images, we develop a coordinate-based method that directly clones in the spherical domain. Our method neither differentiates the polar regions and equatorial regions, nor identifies the boundaries in the unrolled planar-formatted panorama. We discuss in depth two unique issues in panorama cloning, i.e. preserving the patch's orientation, and handling the large-patch cloning (covering over 180° field-of-view) which may suffer from discoloration artifacts. As experimental results demonstrate, our method is able to get visually pleasing cloning results and achieve real time cloning performance.

Keywords: 360° panoramic image, panorama cloning, spherical mean value coordinate (SMVC), stereographic projection, large-patch cloning.

Categories and Subject Descriptors (according to ACM CCS): I.3.3 [Computer Graphics]: Picture/Image Generation—

1. Introduction

Panorama, a wide-angle view representation of a physical scene, has a long history dated back to the 18th century. Rather than being artistic works in early days, panoramic images have became more prevalent in recent years due to the progress of image stitching techniques and spherical imaging system, for displaying landscapes, street side views, or astronomic sceneries. Nowadays, enormous panoramas are publicly available via multiple well-known navigation websites, including Google Street View, Microsoft Bing Map, 360 Cities, etc. The public panoramas usually capture the whole field of view in all directions around the photographer, and most of which also cover up and down views. Due to the embedded sphere geometry, for viewing convenience a 360° panorama is commonly represented in the unrolled latitude-longitude planar format. It shows all the views of the panorama in a way natural to viewers, often with the horizon aligned to the equatorial line in the sphere, yet subjective to increasing distortions near two poles.

Recently there are a number of panorama-based applications emerging, including online street-level virtual navigation [ADF*10, ZWF*13], city-scale change detection [TBP13], scene recognition and view detection [XEOT12], floor-plan construction [RC14] etc. These applications utilize the content in a panorama without image editing or modification. In terms of panoramic image editing, Schröder and Sweldens [SS95] addressed the problem of sharpening and smoothing 360° panoramas via spherical wavelets. Bülow [BÖ4] used spherical harmonic functions to smooth 3D surfaces, which can be regarded as panoramas. Kazhdan and Hoppe [KH10] proposed a panorama enhancement method based on a metric-aware solver. Zhu et al. [ZMH15] proposed a panorama completion method, in which the hole region is filled after it has been warped to 2D plane.

In this paper, we address the problem of image cloning for 360° panoramas, which clones a patch of the source panorama to the target panorama. Traditional methods for planar image cloning typically solve a Poisson equation with Dirichlet boundary condition defined by the target image [PGB03, JSTS06]. The fundamental machinery is to construct a Laplacian membrane that smoothly interpolates the

† lwan@tju.edu.cn

difference between the source and target images along the boundary across the entire cloned region. Later on, an approximation approach based on mean value coordinates was originally proposed in [FHL^{*}09]. Because of its advantages in terms of speed, memory footprint, and parallelizability, the coordinate-based method has been extended in several works [WCPB10, BWS^{*}13, CZSH13].

Considering 360° panorama cloning, an intuitive user interface is to perform the cloning over the latitude-longitude planar format. However, planar image cloning methods are not directly applicable. One major difficulty lies in that we should guarantee the cloned patch to have consistent geometric deformations with the target image wherever the cloned patch is pasted. It is noted that panorama is subjective to the sphere geometry constraint. Hence, we treat the cloned patch as a spherical polygon, and extend the coordinate-based cloning technique to the spherical domain. Our work has three contributions:

1. We are the first to study 360° panorama cloning, a new problem belonging to panorama editing, and get pleasing cloning results.
2. We explain how to preserve the orientation of cloned patches, which is an inherent problem of panorama cloning, with a two-step rotation estimation method.
3. We remove discoloration artifacts when cloned patches cover over 180° field-of-view by a splitting-based method, which is based on our new deduction of spherical mean value coordinates.

2. Related Work

2.1. Panorama-based Applications

By providing wide fields of view far beyond planar images, 360° panoramas have been successfully applied in a number of recent new applications. For instance, online street-level virtual navigation [ADF^{*}10, ZWF^{*}13] synthesizes new panoramas at intermediate views in-between pre-captured ones. City-scale change detection [TBP13] estimates architectural structure changes between a panorama collection and a maintained cadastral 3D model. Xiao et al. [XEOT12] proposed to recognize image scene and view direction based on a large panorama dataset. Micusik and Kosecka [MK09] constructed 3D city model from street-view panoramic sequences. There also exist several works on panorama smoothing and sharpening, using spherical wavelets [SS95], spherical harmonics functions [BÖ4], and metric-aware solver [KH10]. Zhu et al. proposed a panorama completion method for street view images [ZMH15], which needs to warp the hole region to 2D plane first. In this paper, we focus on panorama cloning, a new problem that has not been studied yet to the best of our knowledge.

2.2. Image Cloning

Traditional image cloning methods [PGB03, JSTS06, AH15] eventually solve a large sparse linear system defined by the Poisson equation. Solving the Poisson equation for large cloned patches is a computing and memory intensive task. Although some acceleration algorithms [MP08] were proposed, they are still time consuming for real-time applications.

Coordinate-based techniques [FHL^{*}09, WCPB10] offer practical alternatives for image cloning. These methods diffuse the differences along the patch's boundary to the interior region by interpolation without solving Poisson equations. The widely used diffusion weights are mean value coordinates [FHL^{*}09] and harmonic coordinates [WCPB10]. Coordinate-based methods have nice properties, including high speed, small memory footprint and ease of parallelization. They have recently been extended to video composition [CZSH13] and stereoscopic image cloning [LSC^{*}12]. Our panorama cloning belongs to the coordinate-based technique.

2.3. Mean Value Coordinates

The mean value coordinate [Flo03] motivated by mean value theorem has important properties, such as smoothness, linear independence, and refinability. It can be used to approximate a harmonic-like solution to the boundary interpolation problem, and has many applications in computer graphics [HF06], such as Phong shading for arbitrary polygons, image warping and image cloning [FHL^{*}09].

Many extensions have been made to planar mean value coordinate. Ju et al. [JSW05] generalized mean value coordinates from closed 2D polygons to closed triangular meshes, which are continuous and smooth on the interior of meshes. Langer et al. [LBS06] proposed *spherical mean value coordinate (SMVC)*, which gives the coordinates for point \mathbf{v} located on the unit sphere with respect to a spherical polygon. By replacing the linear precision property of planar coordinates by a requirement in terms of center of mass, [Rus10] introduced a method for defining and computing barycentric coordinates with respect to polygons on general surfaces. Panozzo et al. [PBDSH13] presented an efficient method for computing and inverting weighted averages on surfaces for point on surfaces. Our panorama cloning uses spherical mean value coordinates as diffusion weights because of the embedded sphere geometry.

3. Overview of Spherical Image Cloning

Let $S = \mathbb{S}^2$, $T = \mathbb{S}^2$ be the domain of source and target panoramas, $g : S \rightarrow R$, $f^* : T \rightarrow R$ be the intensities of source and target image. Assume that we want to seamlessly clone the source patch $\Omega_s \subset S$ to the target patch $\Omega_t \subset T$. Similar to the planar image cloning presented by Farbman et

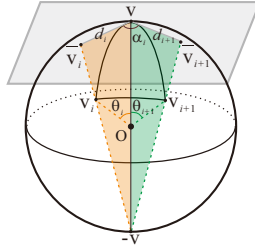


Figure 1: Notation for the deduction of the spherical mean value coordinates, see Appendix A for more details.

al. [FHL*09], the intensity of the point $\mathbf{v} \in \Omega_t$ will be given by

$$f(\mathbf{v}) = g(\mathbf{v}) + \sum_{i=1}^n \lambda_i(\mathbf{v})(f^* - g)(\mathbf{v}_i), \quad (1)$$

where $\lambda_i(\mathbf{v})$ is the spherical mean value coordinates of \mathbf{v} with respect to the boundary of patch Ω_t , whose vertices are $\mathbf{P} = \{\mathbf{v}_1, \dots, \mathbf{v}_n\}$. According to our deduction in Appendix A and [LBS06], $\lambda_i(\mathbf{v})$ is given by

$$\lambda_i(\mathbf{v}) = \frac{(\tan \frac{\alpha_{i-1}}{2} + \tan \frac{\alpha_i}{2}) / \sin \theta_i}{\sum_j \cot \theta_j (\tan \frac{\alpha_{j-1}}{2} + \tan \frac{\alpha_j}{2})}, \quad (2)$$

where θ_i is the angle between \mathbf{v} and \mathbf{v}_i ; α_i is the signed angle between vectors $\mathbf{v} \times \mathbf{v}_i$ and $\mathbf{v} \times \mathbf{v}_{i+1}$ (see Figure 1). Because the mean value interpolant is very smooth away from the boundary of the cloned region, we construct an adaptive mesh for the spherical polygon as in [FHL*09] to avoid much of the computation.

It seems that spherical image cloning is quite similar to planar image cloning. However, we find that it suffers from two unique problems. First, we need to preserve the orientation of the cloned patch after transformation so as to avoid weird appearance. Second, cloning large patches may result in discoloration artifacts, which damage the appearance of the cloned patches seriously. In the next, we will discuss these two issues in details.

4. Preserving Cloned Patch Orientation

Panoramas are usually captured with the horizon aligned with the equatorial line. To compute the intensity difference $f^* - g$ in Equation 1, we need to determine the boundary of the target patch according to the source patch. In planar image cloning, the target patch can be computed by translating the source patch with offset $\mathbf{v}_s - \mathbf{v}_t$, where \mathbf{v}_s is the datum point, e.g. the centroid of the source patch, and \mathbf{v}_t is the specified target cloning position. In spherical image cloning, since \mathbf{v}_s and \mathbf{v}_t are both on the surface of sphere, the transformation between \mathbf{v}_s and \mathbf{v}_t now becomes 3D rotation.

A naive method to compute the 3D rotation is using the

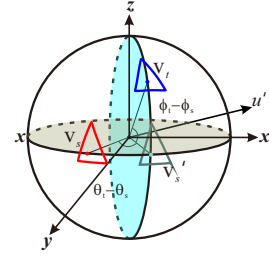


Figure 2: To estimate the rotation between \mathbf{v}_s and \mathbf{v}_t , we first rotate \mathbf{v}_s to make it have the same azimuthal angle with \mathbf{v}_t , then rotate the intermediate point \mathbf{v}_s' to \mathbf{v}_t .

axis-angle representation, which is given by Rodriguez' rotation formula

$$\mathcal{R}(\mathbf{u}, \theta) = I \cos \theta + \sin \theta [\mathbf{u}]_{\times} + (1 - \cos \theta) \mathbf{u} \otimes \mathbf{u}, \quad (3)$$

where $\mathbf{u} = \mathbf{v}_s \times \mathbf{v}_t$ is the rotation axis and $\theta = \arccos(\mathbf{v}_s \cdot \mathbf{v}_t)$ is the rotation angle. However this method may greatly change the orientation of cloned patch, leading to unexpected appearance as shown in Figure 3(c).

Here, we apply a two-step rotation estimation method to preserve the orientation of cloned patch (illustrated in Figure 2). Assume the spherical coordinates of \mathbf{v}_s and \mathbf{v}_t are (ϕ_s, θ_s) and (ϕ_t, θ_t) respectively, where ϕ_s and ϕ_t are azimuthal angles, θ_s and θ_t are polar angles. We first rotate \mathbf{v}_s around z -axis by $\phi_t - \phi_s$ to make it have the same azimuthal angle with \mathbf{v}_t . This rotation is denoted as R_1 , given by

$$R_1 = \begin{bmatrix} \cos(\phi_t - \phi_s) & -\sin(\phi_t - \phi_s) & 0 \\ \sin(\phi_t - \phi_s) & \cos(\phi_t - \phi_s) & 0 \\ 0 & 0 & 1 \end{bmatrix}. \quad (4)$$

The intermediate rotated point has the spherical coordinate (ϕ_t, θ_s) and is denoted as $\mathbf{v}_s' = R_1 \mathbf{v}_s$.

The second step is to transform \mathbf{v}_s' to \mathbf{v}_t . This can be accomplished by rotating \mathbf{v}_s' around the normal \mathbf{u}' of blue-colored plane by $\theta_t - \theta_s$, where

$$\mathbf{u}' = \mathbf{v}_s' \times [0 \ 0 \ 1]^T. \quad (5)$$

This rotation is represented by Rodriguez' rotation formula in Equation 3 as

$$R_2 = \mathcal{R}(\mathbf{u}', \theta_t - \theta_s). \quad (6)$$

Hence, the final rotation R between \mathbf{v}_s and \mathbf{v}_t is the combination of R_1 and R_2 , given by

$$R = R_2 R_1. \quad (7)$$

The cloning results with rotation matrix computed by different methods are shown in Figure 3. We can see that the orientation of the parterre is well preserved by the two-step rotation estimation method.



Figure 3: The cloning results using different methods to compute the rotation matrix: (a) the source panorama and selected cloning patch; (b) the target panorama; (c) cloning result using naive method; (d) cloning result using two-step estimation method.

5. Large Patch Cloning

The basic cloning method works well for small cloning patches, however it inevitably suffers from discoloration artifacts when we want to clone a quite large patch (see the example shown in Figure 4(a)). The main reason is that the spherical mean value coordinate given by Equation 2 “overflows”, when the angle θ_i between point \mathbf{v} and boundary point \mathbf{v}_i is more than 180° . The problem of discoloration artifacts is unique to spherical panorama cloning. Although some previous works [XSMC10, ZT11, CCT*09, CZSH13] observed a similar problem, the artifacts they tackled are caused by large color differences or texture differences, which is not discussed in our paper.

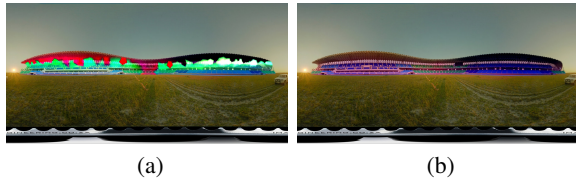


Figure 4: Discoloration artifacts. (a) Discoloration artifacts when the cloned patch covers more than 180° . (b) The artifacts can be removed with splitting-based cloning.

5.1. Analyzing Decoloration Artifacts

From Figure 4 we notice that discolored pixels appear near two ends of the cloned patch, while central pixels have much less artifacts. By further examining the discolored pixels, we find their spherical mean value coordinates (SMVC) have rather large magnitudes. Although we currently have no way to prove this analytically, we try to give an explanation by examining the computation of SMVC.

To facilitate the analysis, we re-deduce SMVC by applying the stereographic projection in Appendix A. Here, we only recall critical relations. Let $\bar{\lambda}_i$ be planar mean value coordinate of one point with respect to the projected polygon, λ_i denotes intermediate coordinate, and λ_i denotes the final spherical mean value coordinate with respect to the spherical polygon. From the deduction, the intermediate coordinate $\bar{\lambda}_i$ is the scaling of $\bar{\lambda}_i$ (Equation A.4), i.e.

$$\bar{\lambda}_i = \frac{2}{1 + \cos \theta_i} \bar{\lambda}_i. \quad (8)$$

The spherical mean value coordinates λ_i is related to $\bar{\lambda}_i$ (Equation A.9) by

$$\lambda_i = \frac{\bar{\lambda}_i}{2 - \sum_i \bar{\lambda}_i}. \quad (9)$$

Figure 5 demonstrates the coordinate values for one central pixel and one discolored pixel (both from Figure 4(a)). For the discolored pixel (the first row of Figure 5), there is one angle θ_i (between \mathbf{v} and boundary point \mathbf{v}_i) very close to π . Due to Equation 8, the corresponding $\bar{\lambda}_i$ is abnormally enlarged as shown in Figure 5(c). In Equation 9, the sum $\sum_i \bar{\lambda}_i$ would be close to 2, e.g. 2.0191 for this exemplar discolored pixel. This makes λ_i be negative and have large magnitude as shown in Figure 5(d). On the contrary, for the central pixel (the bottom row in Figure 5), the angle θ_i is far less than π . The curve of coordinate $\bar{\lambda}_i$ has a similar shape with that of λ_i . As a result, λ_i is the scaling of $\bar{\lambda}_i$ with small factor, and has normal magnitude. For the example in Figure 4(a), the cloned region has a field of view around 300° , and hence the discoloration artifacts seem to appear almost everywhere.

5.2. Splitting-based Cloning

Since no decoloration artifacts occur when θ_i (the angle between the interpolated point and boundary points) is less than 180° , we think about the possibility to constrain the field of view of cloning patches. Encouraged by the fact that the central points in large cloning patches can get normal appearance, we develop a simple solution, by splitting the large cloning patch into two small patches, each of which has less than 180° . In the following, we first derive the modified spherical mean value coordinates.

Suppose the adaptive mesh constructed in the cloned patch is Ω , it is split into two sub-regions Ω_1 and Ω_2 along a path P_c (its selection will be discussed in Section 5.3), as illustrated in Figure 6. Let P denote the boundary of Ω , and $P_1 = \partial\Omega_1$, $P_2 = \partial\Omega_2$ denote the boundaries of the two sub-regions. Then the splitting path can be represented as $P_c = P_1 \cap P_2$. The vertices of the adaptive mesh are separated into two sets $A = \{\mathbf{v} | \mathbf{v} \in \Omega_1\}$ and $B = \{\mathbf{v} | \mathbf{v} \in \Omega_2\}$. For clarity, we introduce two auxiliary variables $P_l = P_1 - P_2$ and $P_r = P - P_l$, which correspond to the sky blue line and the green line in Figure 6. For the vertices $\mathbf{v} \in A \cap B$, i.e. the vertices on the splitting path P_c , their spherical mean

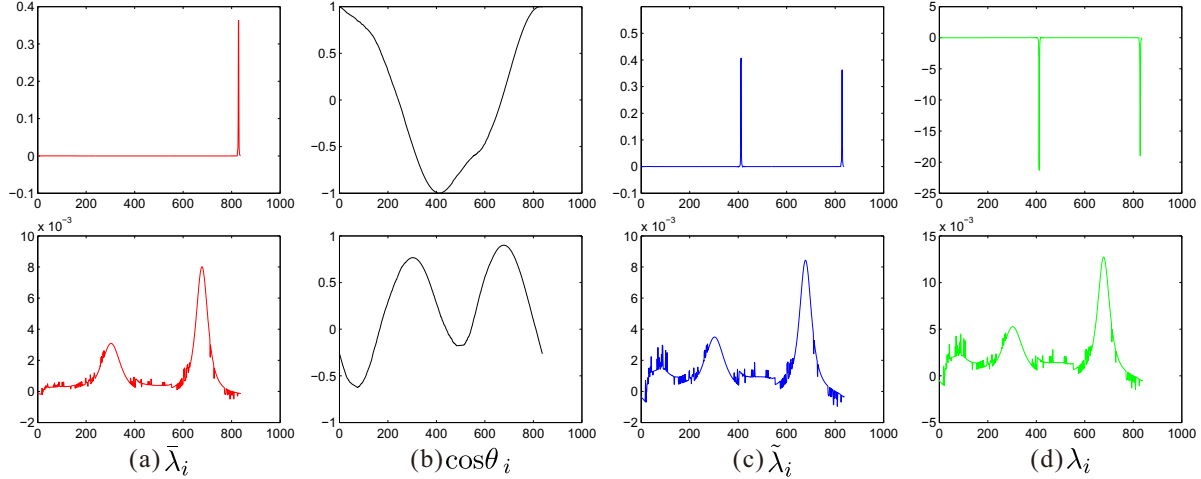


Figure 5: Compared with the central pixels (the second row), the component of the spherical mean value coordinates for the pixels near the ends of the patch may have large absolute values. The horizontal axis represents the indices of pixels on the cloned patch boundary. See text for details.

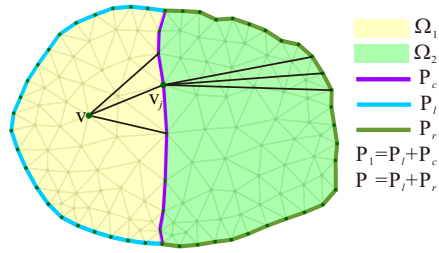


Figure 6: The definition of sub regions and boundaries for splitting-based cloning.

value coordinates can be directly computed with respect to the original spherical polygon boundary P , i.e.

$$\mathbf{v} = \sum_{\mathbf{v}_i \in P} \lambda_{\mathbf{v}_i} \mathbf{v}_i, \text{ if } \mathbf{v} \in P_c, \quad (10)$$

where $\lambda_{\mathbf{v}_i}$ is the spherical mean value coordinate of \mathbf{v} corresponding to \mathbf{v}_i .

For the vertices $\mathbf{v} \in A - B$, i.e. the rest vertices in Ω_1 , we first compute their spherical mean value coordinates with respect to P_l and get

$$\mathbf{v} = \sum_{\mathbf{v}_i \in P_l} \bar{\lambda}_{\mathbf{v}_i} \mathbf{v}_i, \text{ if } \mathbf{v} \in A - B. \quad (11)$$

Because $P_l = P_c \cup P_l$, Equation 11 can be written as

$$\mathbf{v} = \sum_{\mathbf{v}_j \in P_c} \bar{\lambda}_{\mathbf{v}_j} \mathbf{v}_j + \sum_{\mathbf{v}_i \in P_l} \bar{\lambda}_{\mathbf{v}_i} \mathbf{v}_i. \quad (12)$$

By substituting $\mathbf{v}_j \in P_c$ with Equation 10, the above equation

becomes

$$\begin{aligned} \mathbf{v} &= \sum_{\mathbf{v}_j \in P_c} \bar{\lambda}_{\mathbf{v}_j} \sum_{\mathbf{v}_i \in P} \lambda_{\mathbf{v}_j \mathbf{v}_i} \mathbf{v}_i + \sum_{\mathbf{v}_i \in P_l} \bar{\lambda}_{\mathbf{v}_i} \mathbf{v}_i \\ &= \sum_{\mathbf{v}_i \in P} \sum_{\mathbf{v}_j \in P_c} \bar{\lambda}_{\mathbf{v}_j} \lambda_{\mathbf{v}_j \mathbf{v}_i} \mathbf{v}_i + \sum_{\mathbf{v}_i \in P_l} \bar{\lambda}_{\mathbf{v}_i} \mathbf{v}_i. \end{aligned} \quad (13)$$

Since $P = P_l \cup P_r$, we further rewrite Equation 13 as

$$\begin{aligned} \mathbf{v} &= \sum_{\mathbf{v}_i \in P_l} \bar{\lambda}_{\mathbf{v}_i} \mathbf{v}_i + \sum_{\mathbf{v}_i \in P_l} \sum_{\mathbf{v}_j \in P_c} \bar{\lambda}_{\mathbf{v}_j} \lambda_{\mathbf{v}_j \mathbf{v}_i} \mathbf{v}_i \\ &\quad + \sum_{\mathbf{v}_i \in P_r} \sum_{\mathbf{v}_j \in P_c} \bar{\lambda}_{\mathbf{v}_j} \lambda_{\mathbf{v}_j \mathbf{v}_i} \mathbf{v}_i. \end{aligned} \quad (14)$$

Then the coordinates for vertices $\mathbf{v} \in A - B$ with respect to the original spherical polygon boundary P can be expressed as

$$\bar{\lambda}_{\mathbf{v}_i} = \begin{cases} \bar{\lambda}_{\mathbf{v}_i} + \sum_{\mathbf{v}_j \in P_c} \bar{\lambda}_{\mathbf{v}_j} \lambda_{\mathbf{v}_j \mathbf{v}_i}, & \text{if } \mathbf{v}_i \in P_l; \\ \sum_{\mathbf{v}_j \in P_c} \bar{\lambda}_{\mathbf{v}_j} \lambda_{\mathbf{v}_j \mathbf{v}_i}, & \text{if } \mathbf{v}_i \in P_r. \end{cases} \quad (15)$$

These coordinates are used as the weights to diffuse intensity difference when cloning the patch. A similar way can be taken to compute the coordinates for the vertices $\mathbf{v} \in B - A$.

It is worthy pointing out that the coordinates computed by the splitting-based method are different from those computed by the basic method in Section 3. We think the reason is that when computing with respect to different polygons, the tangent and the reciprocal of the distance, both of which are nonlinear functions, will get different values.

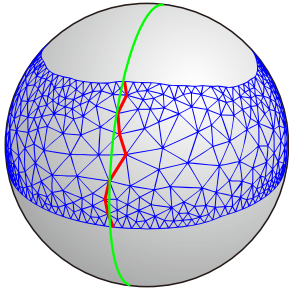


Figure 7: Splitting path computation (see text for more details).

5.3. Splitting Path

The key point for the splitting-based cloning to work is breaking the large patch into two small patches, each covering less than 180°. Because the source patches are selected on the unrolled spherical images, they unlikely cover more than 180° vertically. Accordingly, a safe way to get two reasonable patches is vertically splitting the spherical polygon in the middle.

To be specific, we first find the median of the azimuthal angles of the boundary vertices. Based on it, a great circle that passes through z -axis is constructed (the green curve in Figure 7). We assume that the great circle and the spherical polygon have only two intersection points. Next, we find the boundary vertices nearest to each of the intersection points, and compute the splitting path (marked as the red curve in Figure 7) as the shortest path of mesh points connecting the two boundary vertices. In addition to this splitting path generation method, we have tested another two solutions. As will be discussed in Section 6.3, our current method is easy to compute and able to generate consistently pleasing results.

6. Experimental results

In the experiments, we use images from SUN360 panorama database [XEOT12]. We first compare the cloning results of our method with those generated by planar image cloning, then we show the results generated with and without the splitting when the cloned region covers more than 180°. After discussing the performance of the splitting-based cloning, we give our timing statistics.

6.1. Comparison with Planar Image Cloning

Figure 8 shows the results by our method and the planar image cloning [FHL*09]. Although it is hard to distinguish which results are better in the unfolded latitude-longitude panoramic format, it becomes clearer after mapping onto the sphere. In Figure 8 (a), we replace the lamp of a room with another one. In the result of the planar image cloning method, the original circular lamp becomes elliptical and

the lamp decoration is stretched. On the contrast, our method preserves the lamp shape as well as the decoration. A similar performance is observed in Figure 8 (b), in which the flowerpot in the cloning result of the planar method is extruded, while our result does not suffer from the problem.

Another advantage of our method is that it can naturally circumvent the boundary problem due to the spherical mapping. For the example in Figure 9(a), we clone the inscriptions on the source image to the wall of the target image. When the cloning position gets close to the left boundary of the target spherical image, the cloned region can automatically appear in the right part of the target image with our method. Although the same effect can be achieved by simple tricks in the planar image cloning, it can not deal with the case when the cloning position gets close to the top or bottom boundary of the target image. As shown in Figure 9(b), the planar image cloning results in a much distorted bird in the spherical domain. The main reason is that the left and right boundary of the panorama should be coincided and represent a meridian, while the top and the bottom boundary represent the north and south pole of the sphere respectively.

6.2. Large Patch Cloning

Figure 10 gives some examples of cloned regions covering more than 180° field-of-view. On the first row, we clone a long building between two images. For the result generated by the panorama cloning without splitting, the two wings of the cloned building are discolored and darker than the main part. This is because the target image has higher intensities than the source image, and after we diffuse positive intensity differences with negative weights whose magnitudes are large (see Section 5.2), the intensity becomes very small. For the result generated by the cloning with splitting, the intensity of the cloned region is more smooth, and gives more pleasant appearance.

The second row gives another example, in which the building in the source image is placed on the platform in the target image. Contrasted with the first example, the two ends of this building are brighter than the central part if cloning without splitting. This is due to the fact that the intensity of the target image in this example is lower than that of the source image. As the cloned region is more complicated, if we directly clone the selected patch to the target image, the cloned region will conflict with the surrounding background of the target image. To make them match well, we compute a matte from the source patch, and remove the unwanted part by modulating the cloned region with the matte. The third row in Figure 10 gives one more example that also uses matte modulation.

6.3. Comparing Different Splitting Path Solutions

In the experiments, we observe that the computed coordinates are not equal for different splitting paths. Besides the



Figure 8: Compared with the planar image cloning, our method can preserve the shape of the cloned object: (top) the source panorama and selected cloning regions, (middle) the cloning results using planar image cloning method [FHL*09], (below) the cloning results using our method.

splitting path generation method given in Section 5.3, we consider another two possible solutions and make comparison in the following.

- Alternative 1 performs the PCA on the vertices of the *spherical polygon* P . The first principal component is treated as the direction of the spherical polygon, and induces a great circle, whose normal vector is the principal component. Given the great circle, the splitting path then can be computed as the method given in Section 5.3.
- Alternative 2 performs the PCA on the *projected spherical polygon* \tilde{P} , and the principal component is used to determine a great circle, based on which the splitting path is computed.

The generated splitting paths and their corresponding cloning results are show in Figure 11. We find when the range of the angles that the spherical polygon covers is considerably large, Alternative 1 may give inappropriate splitting path. As demonstrated in Figure 11(c), one sub-region after splitting still covers more than 180° , and so the cloned result suffers from discoloration artifacts. On the other hand, Alternative 2 works well even for the cloned patches that are not horizontal. In our experience, the slanted objects that cover more than 180° are rare. Therefore we choose the method given in Section 5.3, which avoid the PCA operation and is more timing efficient.

6.4. Timing Performance

We test the timing performance on a desktop installed with Intel(R) Core(TM) i5-1330 CPU @ 3.00GHz and NVIDIA GeForce GT 640. Our current implementation constructs the adaptive mesh, computes the spherical mean value coordinate, and evaluates the membrane at each mesh vertex on the CPU. The interpolation of pixels within each triangle of the mesh is performed on the GPU by exploiting the hardware rasterization ability.

Table 1: Performance statistics for panorama cloning: the times for splitting-based cloning are in bold type.

boundary pixels	mesh vertices	cloned pixels	preprocessing time(ms)	cloning time(ms)
279	1031	15009	23	0.342
500	1957	43955	71	0.387
691	2763	77631	140	0.428
			5873	0.434
900	3661	96989	238	0.472
			9804	0.469
1179	4925	186314	419	0.531
			17852	0.535

The timing is recorded as two parts: the preprocessing

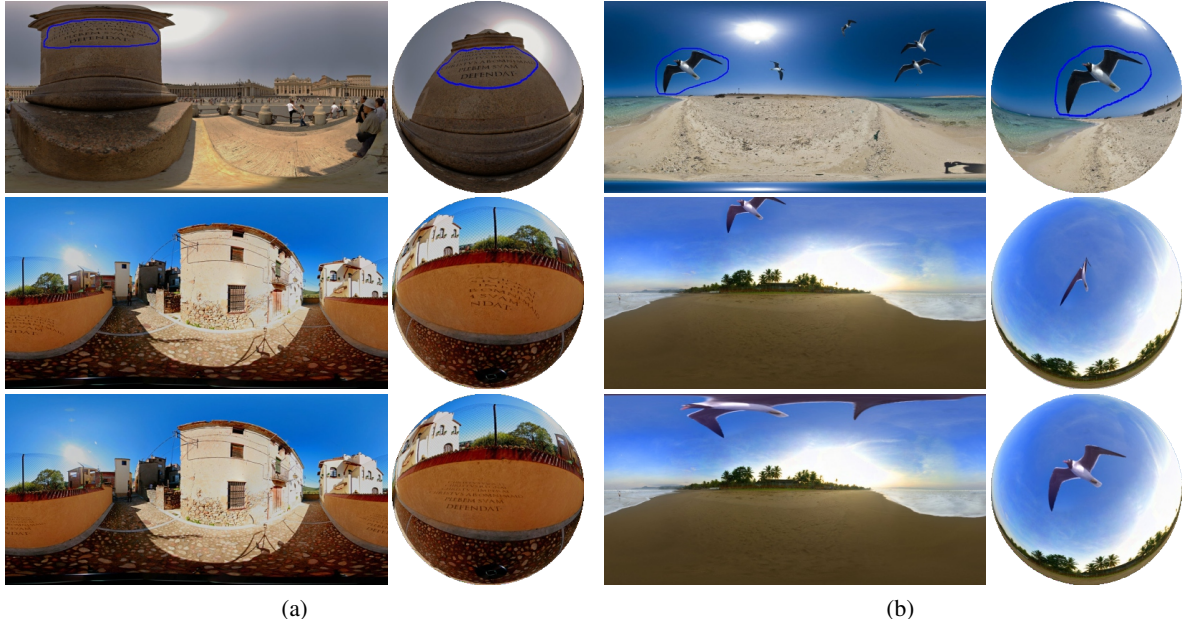


Figure 9: Compared with the planar image cloning [FHL*09], our method does not suffer from the boundary problem when the cloning position gets close to the boundaries of the panorama.

time, which correspond to the steps of adaptive mesh construction, spherical mean value coordinates computation and membrane evaluation; and the cloning time, which corresponds to pixel color interpolation. For a specified cloning patch, the preprocessing procedure is carried out only once for different target cloning positions. Table 1 gives the running time with respect to different number of boundary pixels, adaptive mesh vertices and cloned pixels. For the 3rd to 5th cases, which clone the patches that cover more than 180°, we record the time for cloning without and with splitting (bold type). From the table we can see that as the number of boundary pixels and adaptive mesh vertices increases, more time is required for the preprocessing procedure. Although the cloning time increases as the cloned regions become larger, this part of time is relatively short. Another fact is that cloning with splitting takes much more preprocessing time than that without splitting, which seriously affects the timing performance.

Note that because panoramas are oversampled near poles, if we clone a patch near the equator of the source panorama to the polar regions of the target panorama, the cloned patch can be obviously blurred. Supersampling is used to deal with this problem, and Table 2 shows the cloning times for different supersampling configurations when there are about 510 boundary pixels and 1970 adaptive mesh vertices. The cloning time without supersampling is the same to that of the 2nd case in Table 1, in which the test cases are performed without supersampling. Table 2 shows that the cloning time for 2×2 supersampling is approximate to that without super-

sampling. When more samples are used, the cloning time is increased accordingly. Although it needs about 5ms to render a frame for 16×16 supersampling, it can still clone the patch in real time. Actually for quality, the results shown in this paper are generated using this configuration.

Table 2: Performance statistics for different supersampling configuration

supersampling	1×1	2×2	4×4	8×8	16×16
cloning time(ms)	0.387	0.391	0.650	1.687	5.055

7. Conclusion

In this paper, we propose a coordinate based algorithm to solve the problem of 360° panorama cloning, which has not been studied previously. In our work, we re-derive spherical mean value coordinates (SMVCs), and use SMVCs as the weights to achieve panorama cloning. To preserve the orientation of the cloned patch, we develop a two-step rotation computation method. A splitting-based method is proposed to remove discoloration artifacts for the case when cloning large patches cover more than 180° field-of-view. With the proposed method, we can get satisfactory results and achieve real time cloning performance. As one future improvement, we would like to port the computation of SMVC and the evaluation of mean value coordinate membrane to the GPU.

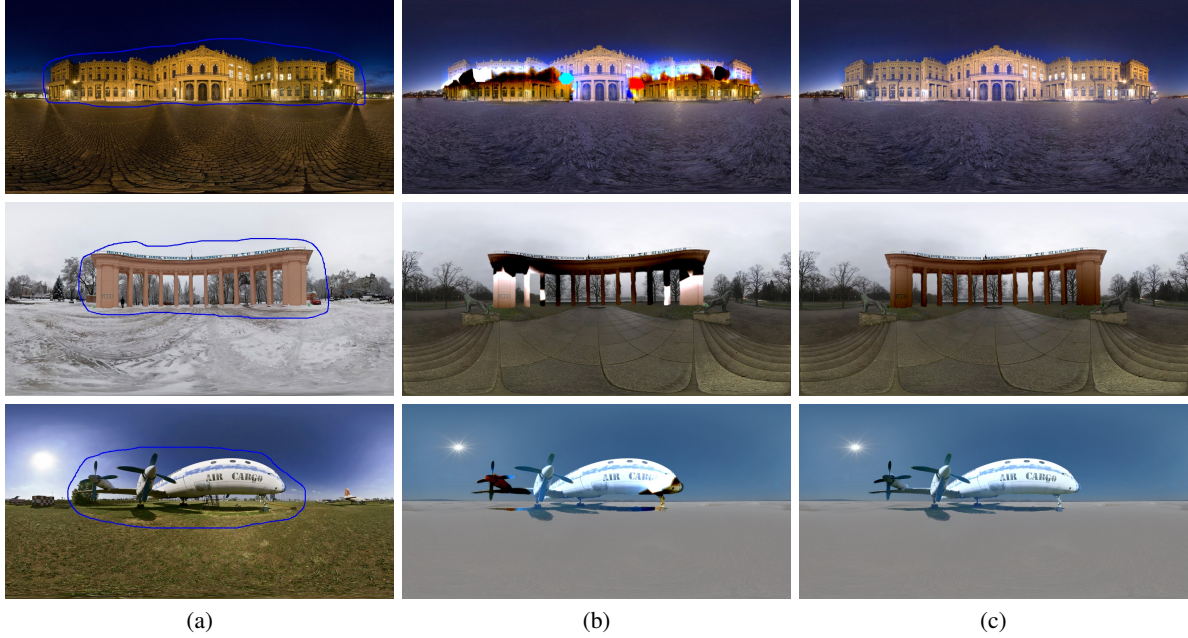


Figure 10: When the cloned patch covers more than 180° (a), the cloning directly using spherical mean value coordinates will cause discoloration artifacts (b). Our splitting-based method can deal with this problem (c).

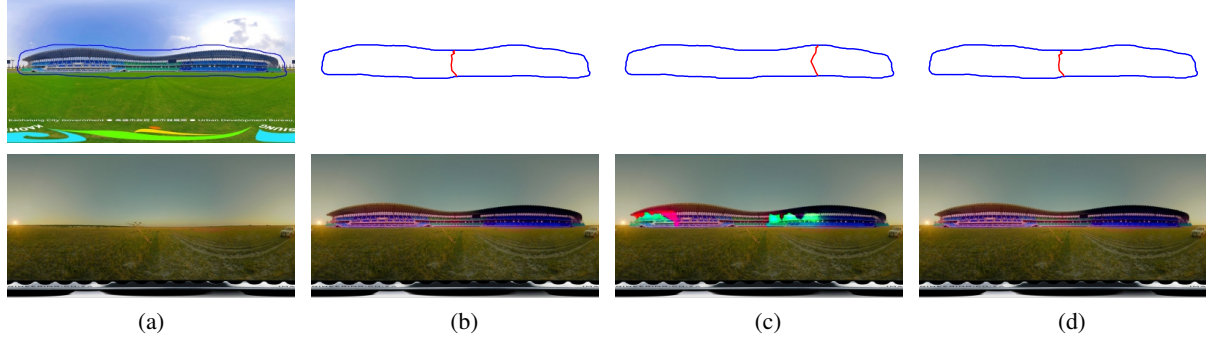


Figure 11: The splitting paths and corresponding cloning results: (a) the source and target panoramas, (b) the splitting path from the method given in Section 5.3, (c) the splitting path computed by performing PCA on the boundary of the spherical polygon (Alternative 1) and (d) the splitting path computed by performing PCA on the boundary of the projected spherical polygon (Alternative 2).

Appendix A: Spherical Mean Value Coordinates

The basic idea to compute spherical mean value coordinates of point \mathbf{v} is first projecting the spherical polygon P to the tangent plane of unit sphere at \mathbf{v} to get a planar polygon \bar{P} , then computing planar mean value coordinates of \mathbf{v} respect to \bar{P} , followed by an anisotropic scaling. To project the spherical polygon, Langer et al. [LBS06] use gnomonic projection, which would project two antipodal points to the same point on the tangent plane. In our work, we use the *generalized stereographic projection* to deduce the spherical mean value coordinates. The main advantage of stereographic projection over gnomonic projection is that except for the projection point, it can project the entire sphere onto a plane without introducing overlapping. Particularly, this new deduction is helpful to analysis the decoloration problem.

As illustrated in Figure 1, we first move the origin of the 3D coordinate system from the sphere center to the projection point, which is the antipodal point of \mathbf{v} and noted as

$$\hat{\mathbf{v}} = -\mathbf{v}. \quad (\text{A.1})$$

In the translated coordinate system, the boundary vertices \mathbf{v}_i of spherical polygon, its projected counterpart $\bar{\mathbf{v}}_i$ and point \mathbf{v}

are represented by

$$\mathbf{v}'_i = \mathbf{v}_i - \hat{\mathbf{v}}, \bar{\mathbf{v}}'_i = \bar{\mathbf{v}}_i - \hat{\mathbf{v}}, \mathbf{v}' = \mathbf{v} - \hat{\mathbf{v}}. \quad (\text{A.2})$$

Following 2D mean value coordinate definition, the planar mean value coordinates of \mathbf{v}' with respect to the projected polygon $\tilde{\mathbf{P}}' = \{\bar{\mathbf{v}}'_1, \dots, \bar{\mathbf{v}}'_n\}$ are given by

$$\tilde{\lambda}_i = \frac{w_i}{\sum_j w_j}, w_i = \frac{\tan \frac{\alpha_{i-1}}{2} + \tan \frac{\alpha_i}{2}}{d_i}, \quad (\text{A.3})$$

where α_i is the signed angle between vectors $\mathbf{v}' \times \mathbf{v}'_i$ and $\mathbf{v}' \times \mathbf{v}'_{i+1}$, and the distance $d_i = \|\bar{\mathbf{v}}'_i - \mathbf{v}'\|$ as shown in Figure 1. Because each $\bar{\mathbf{v}}'_i$ is a scaling of \mathbf{v}'_i , the coordinate $\tilde{\lambda}_i$ of \mathbf{v}' with respect to the spherical polygon $\mathbf{P}' = \{\mathbf{v}'_1, \dots, \mathbf{v}'_n\}$ (in the translated coordinate system) can be constructed from $\tilde{\lambda}_i$, i.e.,

$$\tilde{\lambda}_i = \frac{\|\bar{\mathbf{v}}'_i\|}{\|\mathbf{v}'_i\|} \tilde{\lambda}_i = \frac{2}{1 + \cos \theta_i} \tilde{\lambda}_i, \quad (\text{A.4})$$

where θ_i is the angle between \mathbf{v} and \mathbf{v}_i . What's more, the coordinate $\tilde{\lambda}_i$ defined in Equation A.4 satisfies

$$\sum_i \tilde{\lambda}_i \mathbf{v}'_i = \mathbf{v}'. \quad (\text{A.5})$$

Note that the current computation is operated in the translated coordinate system (originated at $-\hat{\mathbf{v}}$), while our goal is computing the spherical mean value coordinate λ_i of point \mathbf{v} with respect to the spherical polygon \mathbf{P} (in the original coordinate system centered at sphere center), which should satisfy

$$\sum_i \lambda_i \mathbf{v}_i = \mathbf{v}. \quad (\text{A.6})$$

Substituting \mathbf{v}'_i and \mathbf{v}' with Equation A.2, Equation A.5 becomes

$$\sum_i \tilde{\lambda}_i (\mathbf{v}_i + \hat{\mathbf{v}}) = 2\mathbf{v}, \quad (\text{A.7})$$

which can be further rewritten as

$$\sum_i \tilde{\lambda}_i \mathbf{v}_i = (2 - \sum_i \tilde{\lambda}_i) \hat{\mathbf{v}}. \quad (\text{A.8})$$

By comparing Equation A.6 with the above equation, we can get

$$\lambda_i = \frac{\tilde{\lambda}_i}{2 - \sum_i \tilde{\lambda}_i}. \quad (\text{A.9})$$

By using Equation A.3, A.4 and A.9 in addition to some trigonometric identities, the spherical mean value coordinates will have the final form as

$$\lambda_i(\mathbf{v}) = \frac{(\tan \frac{\alpha_{i-1}}{2} + \tan \frac{\alpha_i}{2}) / \sin \theta_i}{\sum_j \cot \theta_j (\tan \frac{\alpha_{j-1}}{2} + \tan \frac{\alpha_j}{2})}. \quad (\text{A.10})$$

References

- [ADF*10] ANGUELOV D., DULONG C., FILIP D., FRUEH C., LAFON S., LYON R., OGALE A., VINCENT L., WEAVER J.: Google Street View: Capturing the world at street level. *Computer* 43, 6 (2010), 32–38. 1, 2
- [AH15] AFIFI M., HUSSAIN K. F.: MPB: A modified poisson blending technique. *Computational Visual Media* 1, 4 (2015), 331–341. 2
- [BÖ4] BÜLOW T.: Spherical diffusion for 3d surface smoothing. *IEEE Transactions on Pattern Analysis and Machine Intelligence* 26, 12 (2004), 1650–1654. 1, 2
- [BWS*13] BIE X., WANG W., SUN H., HUANG H., ZHANG M.: Intent-aware image cloning. *The Visual Computer* 29, 6 (2013), 599–608. 2
- [CCT*09] CHEN T., CHENG M.-M., TAN P., SHAMIR A., HU S.-M.: Sketch2photo: Internet image montage. In *ACM SIGGRAPH Asia* (2009), pp. 124:1–124:10. 4
- [CZSH13] CHEN T., ZHU J.-Y., SHAMIR A., HU S.-M.: Motion-aware gradient domain video composition. *IEEE Transactions on Image Processing* 22, 7 (2013), 2532–2544. 2, 4
- [FHL*09] FARBMAN Z., HOFFER G., LIPMAN Y., COHEN-OR D., LISCHINSKI D.: Coordinates for instant image cloning. In *ACM SIGGRAPH* (2009), pp. 67:1–67:9. 2, 3, 6, 7, 8
- [Flo03] FLOATER M. S.: Mean value coordinates. *Computer Aided Geometric Design* 20, 1 (2003), 19 – 27. 2
- [HF06] HORMANN K., FLOATER M. S.: Mean value coordinates for arbitrary planar polygons. *ACM Transactions on Graphics* 25, 4 (2006), 1424–1441. 2
- [JSTS06] JIA J., SUN J., TANG C.-K., SHUM H.-Y.: Drag-and-drop pasting. In *ACM SIGGRAPH* (2006), pp. 631–637. 1, 2
- [JSW05] JU T., SCHAEFER S., WARREN J.: Mean value coordinates for closed triangular meshes. *ACM Trans. Graph.* 24, 3 (2005), 561–566. 2
- [KH10] KAZHDAN M., HOPPE H.: Metric-aware processing of spherical imagery. In *ACM SIGGRAPH Asia* (2010), pp. 149:1–149:10. 1, 2
- [LBS06] LANGER T., BELYAEV A., SEIDEL H.-P.: Spherical barycentric coordinates. In *Proceedings of the Fourth Eurographics Symposium on Geometry Processing* (2006), pp. 81–88. 2, 3, 9
- [LSC*12] LUO S.-J., SHEN L.-C., CHEN B.-Y., CHENG W.-H., CHUANG Y.-Y.: Perspective-aware warping for seamless stereoscopic image cloning. In *ACM SIGGRAPH Asia* (2012), pp. 182:1–182:8. 2
- [MK09] MICUSIK B., KOSECKA J.: Piecewise planar city 3d modeling from street view panoramic sequences. In *CVPR* (2009), pp. 2906–2912. 2
- [MP08] MCCANN J., POLLARD N. S.: Real-time gradient-domain painting. In *ACM SIGGRAPH* (2008), pp. 93:1–93:7. 2
- [PBDH13] PANOCZO D., BARAN I., DIAMANTI O., SORKINE-HORNUNG O.: Weighted averages on surfaces. *ACM Trans. Graph.* 32, 4 (2013), 60:1–60:12. 2
- [PGB03] PÉREZ P., GANGNET M., BLAKE A.: Poisson image editing. In *ACM SIGGRAPH* (2003), pp. 313–318. 1, 2
- [RC14] RICARDO CARBRAL Y. F.: Piecewise planar and compact floorplan reconstruction from images. In *CVPR* (2014). 1
- [Rus10] RUSTAMOV R. M.: Barycentric coordinates on surfaces. *Computer Graphics Forum* 29, 5 (2010), 1507–1516. 2
- [SS95] SCHRÖDER P., SWELDENS W.: Spherical wavelets: Texture processing. *Eurographics*. 1995, pp. 252–263. 1, 2
- [TBP13] TANEJA A., BALLAN L., POLLEFEYS M.: City-scale change detection in cadastral 3d models using images. In *CVPR* (2013), pp. 113–120. 1, 2

- [WCPB10] WANG R., CHEN W.-F., PAN M.-H., BAO H.-J.: Harmonic coordinates for real-time image cloning. *Journal of Zhejiang University SCIENCE C* 11, 9 (2010), 690–698. [2](#)
- [XEOT12] XIAO J., EHINGER K., OLIVA A., TORRALBA A.: Recognizing scene viewpoint using panoramic place representation. In *CVPR* (2012), pp. 2695–2702. [1](#), [2](#), [6](#)
- [XSMC10] XIE Z.-F., SHEN Y., MA L.-Z., CHEN Z.-H.: Seamless video composition using optimized mean-value cloning. *The Visual Computer* 26, 6 (2010), 1123–1134. [4](#)
- [ZMH15] ZHU Z., MARTIN R. R., HU S.-M.: Panorama completion for street views. *Computational Visual Media* 1, 1 (2015), 49–57. [1](#), [2](#)
- [ZT11] ZHANG Y., TONG R.: Environment-sensitive cloning in images. *The Visual Computer* 27, 6 (2011), 739–748. [4](#)
- [ZWF*13] ZHAO Q., WAN L., FENG W., ZHANG J., WONG T.-T.: Cube2video: Navigate between cubic panoramas in real-time. *IEEE Transactions on Multimedia* 15, 8 (2013), 1745–1754. [1](#), [2](#)